

This is a repository copy of *Numerical calculation of wear in rolling contact based on the Archard equation: Effect of contact parameters and consideration of uncertainties*.

Version: Accepted Version

---

**Article:**

Liu, B., Bruni, S. and Lewis, R. [orcid.org/0000-0002-4300-0540](https://orcid.org/0000-0002-4300-0540) (2022) Numerical calculation of wear in rolling contact based on the Archard equation: Effect of contact parameters and consideration of uncertainties. *Wear*, 490-491. 204188. ISSN 0043-1648

<https://doi.org/10.1016/j.wear.2021.204188>

---

Article available under the terms of the CC-BY-NC-ND licence (<https://creativecommons.org/licenses/by-nc-nd/4.0/>).

**Reuse**

This article is distributed under the terms of the Creative Commons Attribution-NonCommercial-NoDerivs (CC BY-NC-ND) licence. This licence only allows you to download this work and share it with others as long as you credit the authors, but you can't change the article in any way or use it commercially. More information and the full terms of the licence here: <https://creativecommons.org/licenses/>

# Numerical calculation of wear in rolling contact based on the Archard equation

Binbin Liu<sup>1</sup>, Stefano Bruni<sup>1</sup> and Roger Lewis<sup>2</sup>

<sup>1</sup> Dipartimento di Meccanica, Politecnico di Milano, Milano, Italy

<sup>2</sup> Department of Mechanical Engineering, The University of Sheffield, Sheffield, UK

**Abstract:** Wear in rolling contact is a complex phenomenon because it is multi-scale and multi-physical by nature and involves many strongly correlated parameters. It makes the numerical calculation of wear very challenging. In order to simulate wear, a better understanding of the influencing parameters involved in the wear calculation is of importance. This work presents a new numerical calculation of railway wheel wear based on Archard's equation combined with a spatial statistic approach called the Universal Kriging technique. The influence of factors, such as the contact mechanics model and the wear coefficient were studied through numerical experiments. The outcomes provide a new insight into the roles of the contact modelling and of the uncertainties of the wear coefficient in the numerical calculation of wear under various contact conditions. By considering the uncertainties of the wear coefficient, the approach provides a min.-max. range for wear estimation instead of a single deterministic; furthermore, it can provide a detailed wear distribution over the contact patch for damage analysis. In combination with an accurate model of wheel-rail contact, this new wear model offers a more realistic wear prediction compared to the methods presently used for wheel wear estimation in railway vehicles.

**Keywords:** wheel-rail contact, rolling contact, wear coefficient, wear, uncertainty

## 1. Introduction

Prediction of wear evolution due to rolling contact is of great interest in mechanical engineering because it is highly relevant to the cost of maintenance in a wide range of mechanical systems and, if not properly managed, may lead to the failure of the system. The rolling contact phenomenon is common in industrial machinery such as rollers on a cam, rolling contact bearings and wheel-rail contact of railway vehicles. Wear occurring under rolling-sliding contact conditions is a complex phenomenon because it is multi-scale and multi-physical by nature depends on many factors, such as contact geometry, material hardness and roughness, third-body materials, normal and tangential stress distribution at the contact interface [1]. This complexity results from the large number of strongly correlated parameters which means numerical simulation is highly challenging. Therefore, the understanding the influence of parameters involved in wear calculation is of great importance in view of establishing proper models for the wear process in mechanical systems, which is one of the motivations of the current work.

Many attempts have been made to estimate wear due to rolling contact in various fields [2-11]. A recent review on the simulation of wear in different mechanical components can be found in [12]. A significant number of these studies [5-11] sought to predict railway wheel wear which is also the focus of this study. The core of a wear simulation model for rolling contact is the wear law that establishes the relationship between the contact parameters and the material removal. The wear laws applied to the prediction of the

railway wheel wear are mainly the T-Gamma energy approach [5-8] and Archard's equation [9-11]. However, it is worth noting that the uncertainty caused by the parameters involved in Archard's equation has a considerable influence on the results. The contact model that provides contact parameters and wear coefficient are the two most significant influence factors among others.

The importance of the contact model in the calculation of wear has been highlighted and studied extensively in the scientific literature. Early work on the prediction of wear for the wheel-rail system is due to Pearce and Sherratt [5] where a global approach without considering the contact patch information was employed to simplify the simulation. To improve the accuracy of the calculation on the one hand and maintain high computational efficiency, the Hertz theory combined with FASTSIM [13] was used to solve the wheel-rail contact problem locally in the following works [8-10]. A more elaborate local contact model CONTACT [14] was used for railway wheel wear prediction [7,15,16], but this approach turns out to be very time consuming. The use of non-Hertzian contact models for wheel wear simulation was investigated in [15,16], and discrepancies were observed between Hertzian and non-Hertzian models in certain conditions. It is commonly accepted that using Hertz theory and FASTSIM for contact modelling is a good compromise between the calculation efficiency and accuracy for railway wheel wear simulation [16]. However, it should be noted that multiple variants of the FASTSIM algorithm have been proposed [13,17]. To better understand the influence of these variants on wear calculation, a discussion on this algorithm is provided in Section 2 of this paper and numerical simulation results are presented in Section 3.

The wear coefficient is generally derived from laboratory tests with twin-disc test rigs [8-10,18,19]. The obtained values are affected by the testing conditions of the experiment and by the properties of the materials tested. The wear coefficients can be presented in a form of a map where it can be a function of many variables (continuous and discrete), e.g. velocity, load, temperature, dry, and third-body contaminant. Therefore, for a given material pair, a set of wear maps is needed to systematically define the wear behaviour [19]. For the wheel-rail contact, a few wear maps exist presenting the wear coefficient as a function of the contact pressure and the slip velocity concerning different rail and wheel material combinations [9,18,20,21]. The available wear maps are mostly for dry conditions and were obtained from a limited number of experiments because the experimental determination of the wear coefficient is difficult and requires a large experimental effort. Moreover, the accuracy of the available wear maps is affected by limitations in the range of tested values for parameters such as contact pressure, slip velocity. However, this situation is expected to be improved by considering the wear coefficient as an uncertain parameter instead of a deterministically defined value, as is commonly treated now. To this end, a spatial statistic approach called Universal Kriging technique [22] is applied in this work to consider the uncertainty of the wear coefficient obtained from experiments. The application of this technique to an experimental wear map is presented in Section 2 and the numerical prediction of wheel wear obtained using this approach is compared to the one obtained from the traditional deterministic method in Section 3. Finally, some conclusions are proposed in Section 4.

## 2. Archard's equation

Holm [23] introduced the concept of wear volume per sliding distance  $Q$  being proportional to the normal load  $N$  for each material pair according to the following equation:

$$Q = K \frac{N}{H} \quad (1)$$

where  $H$  is the hardness and  $K$  is the wear coefficient which was interpreted as number of removed atoms per atomic collision. Archard improved the theory behind equation (1), which is known as the Archard wear equation [24,25]. It states that the volume of material worn  $V_w$  is proportional to the sliding distance  $d$  and the normal load  $N$ , and inversely proportional to the hardness of the material concerned  $H$ , namely

$$V_w = K \frac{Nd}{H} \quad (2)$$

It is worth noting that different versions of equation (2) may be found in the literature due to different interpretations of the wear coefficient. In equation (2), the wear coefficient  $K$  is predicted as one third for a single hemi-spherical particle and is interpreted as the proportion of all the asperity contacts which results in the production of a worn particle [24], which is dimensionless since the unit of the hardness is  $\text{N/mm}^2$ . It should be recognized that the wear coefficient is not a constant value, but is a possible value in the range of wear rate and must be always be less than unity[26].

In the numerical calculation, the discretized form of the wear depth  $h$  at the centre of each discretized cell  $(x, y)$  of the contact area derived from equation (2) is commonly used as follows:

$$h(x, y) = \frac{K(x,y)p(x,y)v(x,y)\Delta x_{i,j}}{HV_0} \quad (3)$$

where the subscripts  $i$  and  $j$  represent the indices of cell  $(x, y)$  within the contact area,  $p$  is the contact pressure,  $v$  is the sliding velocity,  $\Delta x$  is the length of the cell in the rolling direction, and  $V_0$  is the relative rolling velocity as shown in Fig.1 for a Hertzian contact.

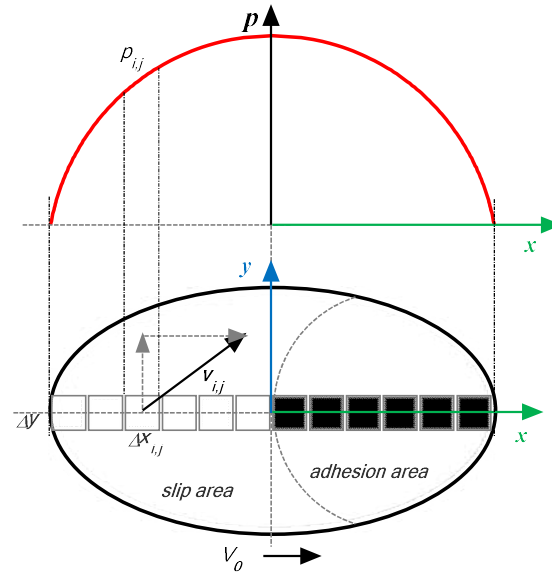


Fig.1 Discretization of the contact patch produced by rolling-sliding contact.

It is clearly shown in equation (3) that the wear coefficient and the contact parameters, i.e. the contact pressure, and the slip velocity, are the governing variables in a wear calculation when using Archard's equation. Therefore, a reliable contact model that determines the contact pressure and slip is crucial for numerical wear calculation. The available approaches to determining these parameters as well as their influences on the estimate of wear will be addressed in detail in the following sections.

## 2.1 Wear coefficient

Among many experimental investigations on the determination of the wear coefficient in the wheel-rail system, the work done by the Royal Institute of Technology (KTH) is worth mentioning. They assume the wear coefficient  $K$  is a function of the slip velocity and contact pressure between the contact pair. The observation from tests shows that the relationship between  $K$  and the slip velocity and contact pressure is also dependent on material and contact conditions (e.g. dry, wet). Therefore, they constructed a wear map based on the analysis and interpolation of different sets of experimental data, including twin-disc and pin-on-disc results, under dry contact conditions, as shown in Fig.2. These treatments attempt to make the wear coefficient somewhat material-independent but introduce an approximation simultaneously, and it is only applicable for dry conditions.[27] Nevertheless, this map is widely used by the railway research community [9-11,28]. It should be noticed that the wear coefficient from the KTH wear map (see Fig.2) must be recalibrated for any specific application to obtain more realistic results compared with measurements [28,29].

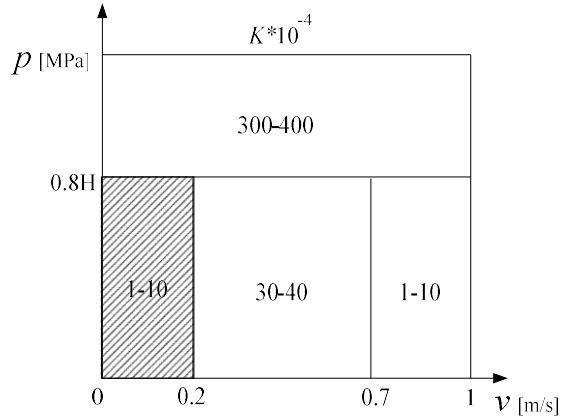


Fig.2. KTH wear map for dry wheel-rail contact adapted from [9].

One difficulty with using the KTH wear map is that in each region of the map a range of values is provided for the wear coefficient  $K$ , instead of a single value. The most common method to determine a single value of the wear coefficient from the KTH map is taking the mean value of the range [10], which is called MV method hereafter. This method is simple, but leads to an averaging effect in the process of a wear calculation and of course no uncertainty is considered at all.

To take the experimental uncertainties in the identification process of the wear coefficient and overcome the problem of having limited measurements, a spatial statistic technique (Universal Kriging technique) [22] is used to determine  $K$  to take advantage of the spatial dependence of measures in the slip velocity and contact pressure plane. A brief description of this method is given in this section. For more details, the interested reader is referred to [30]. The measurements were mapped by Lewis and Olofsson in [18]. The experimental data for Class D wheel combined with rails with different materials, namely BS11, UICA, UICB and 1%Chr under dry condition were chosen for this study as presented in Fig.3.

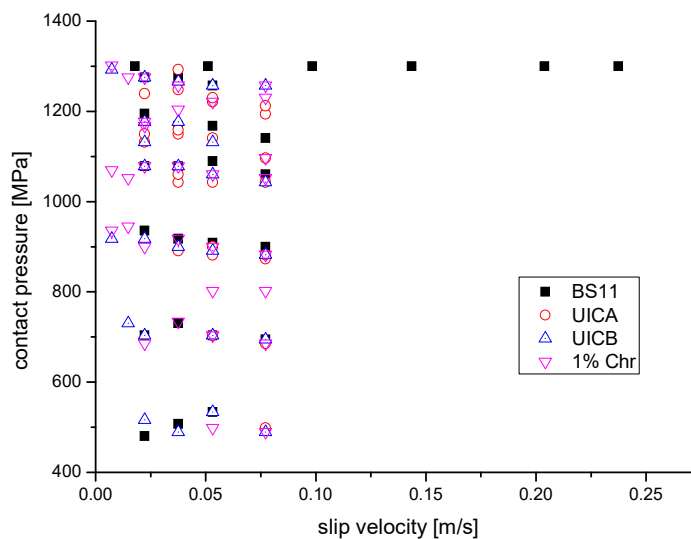


Fig.3. Measurement data distribution.

It can be found that most of the measurements are in the range of 400-1300 MPa for pressure and 0.00-0.08 m/s for slip velocity which fall into the shaded region in Fig.2 considering the hardness of the wheel is constant  $H=2500 \text{ N/mm}^2$ . Only a few measurements belong to the more extreme regime for BS11 rail. Therefore, the wear coefficient is estimated by using a spatial model with linear drift, exploiting the similarities among different materials and the spatial dependence of measurements [30]. Considering that the Universal Kriging method is chosen for prediction and uncertainty analysis of the wear coefficient, it is called UK method in the current paper. The representative results obtained based on the measurement for the rail materials of BS11 and UICA are reported in Fig.4.

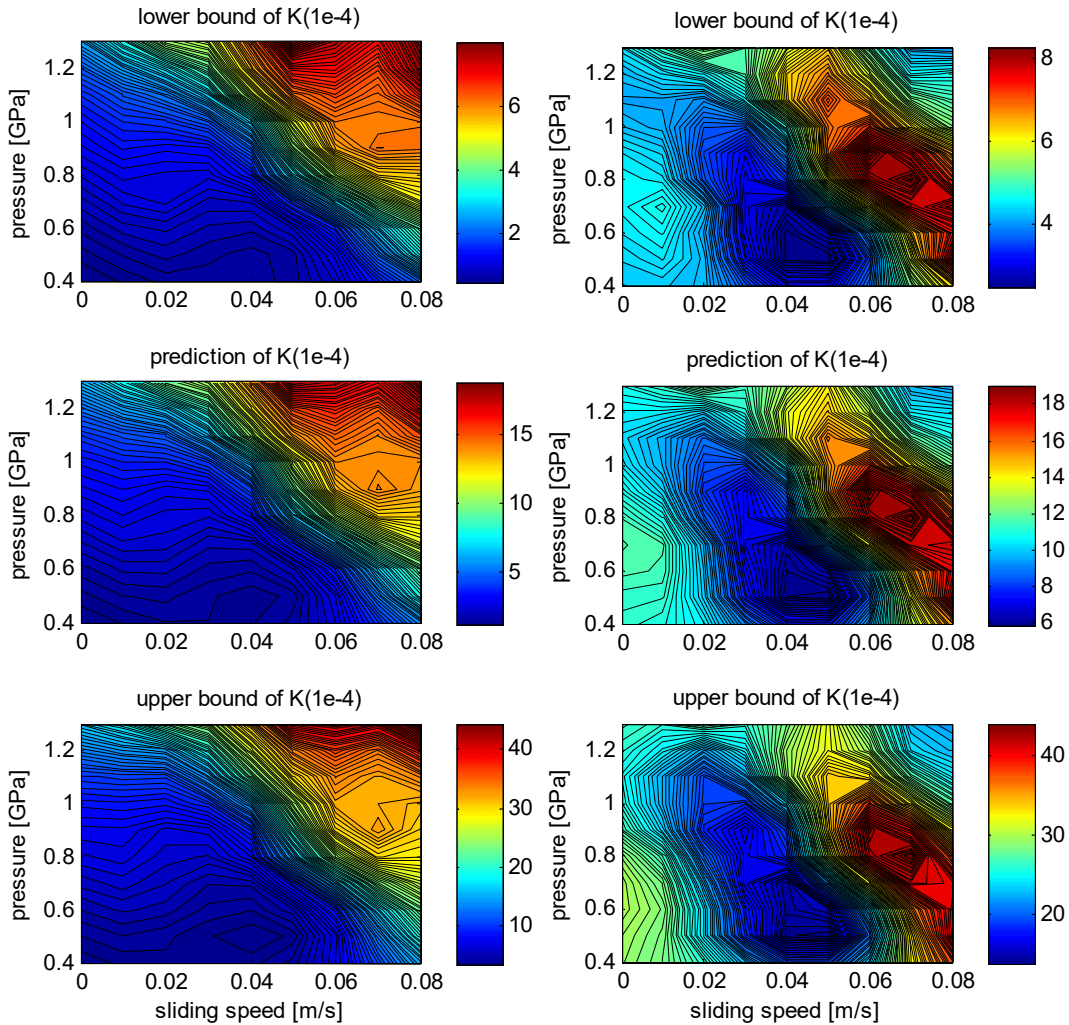


Fig.4. Wear coefficient maps for BS11 (left), UICA (right) in the region with most measures.

It can be observed from Fig.4 that the wear coefficient exhibits clear transitions in the wear map for different material combinations. The KTH wear map is qualitatively acceptable because the wear coefficient distribution for different wheel and rail material combinations shows a similar pattern. However, it must be recalibrated for quantitative estimation of wear for any specific contact pair due to the statistically significant difference that exists. This result has confirmed that the relationship between wear coefficient and the slip

velocity and contact pressure is material-dependent. Therefore, it is unrealistic to use deterministic wear coefficients for various wheel and rail combinations without considering the uncertainty. It is important to notice that the UK method provides the lower and upper bound prediction intervals [30] which is more highly informative than the wear map in Fig.2. In addition, the UK method provides a prediction interval for  $K$  associated to each choice of  $v$  and  $p$  instead of a single determined prediction. As a consequence, this method can be used to predict a range for the amount of material removal, which is more tangible in wheel-rail contact wear prediction. It can also be found that accurate velocity and pressure are crucial to correctly determine the wear coefficient, especially, when the UK method is used. It should be mentioned that the accuracy of the UK method depends on the scope and variety of the experiment data available.

## 2.2 Contact pressure

The determination of the contact pressure and the contact area is generally classified as a normal contact problem. The Hertz theory is widely used for solving this problem, which assumes the contact patch is always elliptical, with semi-axes  $a$  and  $b$  in the rolling and lateral directions, and consequently the contact pressure is treated as semi-ellipsoidal:

$$p(x, y) = \frac{3N}{2\pi ab} \left( 1 - \left( \frac{x}{a} \right)^2 - \left( \frac{y}{b} \right)^2 \right)^{1/2} \quad (4)$$

However, the Hertzian assumption is not always fulfilled or adequate, for example in the context of the wheel-rail contact which frequently produces non-elliptic contact shapes. A more advanced contact model is required for non-elliptic contact conditions, especially for the damage analysis of the wheel-rail system, e.g. wear, rolling contact fatigue and corrugation. The significant difference caused by the non-elliptic contact modelling with respect to Hertzian approach in wheel wear simulation has been reported in [15,16].

The most elaborate contact model to date can be established by a finite element method [31] which is not suitable for wear calculation due to its high computation requirement. The boundary element method such as CONTACT is less expensive, but still requires a significant computational effort which can be problematic when the solution of many contact cases is required, as happens e.g. in the prediction of railway wheel profile evolution due to wear. As a compromise, the so-called approximate non-Hertzian contact method [32-34] is generally considered as best suited for both local contact analysis and online dynamics simulation.

## 2.3 Slip velocity

In order to determine the slip velocity distribution over the contact area, the tangential contact problem has to be solved. CONTACT is qualified for this purpose, but its computational efficiency restricts its application to wear simulation where fast solver is much preferable as mentioned above. The FASTSIM algorithm based on the simplified theory is widely used as an alternative for its high calculation efficiency. It is called simplified theory because it is assumed the displacement at one point within the contact

area is simply proportional and confined only to the stress produced at the same point, as follows:

$$\mathbf{u} = L\boldsymbol{\tau} \quad (5)$$

where  $\mathbf{u}=(u_x, u_y)$  is the displacement vector,  $\boldsymbol{\tau}=(\tau_x, \tau_y)$  is the stress vector, and  $L$  is called the flexibility parameter. It is determined by Kalker by relating the FASTSIM results to those of the linear theory for rolling contact [35]. Three flexibility parameters are obtained, as expressed in equation (6)

$$L_\xi = \frac{8a}{3C_{11}G}, \quad L_\eta = \frac{8a}{3C_{22}G}, \quad L_\varphi = \frac{\pi a\sqrt{a/b}}{4C_{23}G} \quad (6)$$

where  $C_{ij}$  are the Kalker coefficients  $i, j \in \{1,2,3\}$ , and  $G$  is the material shear modulus. The three parameters correspond to longitudinal creepage, lateral creepage and spin respectively. This method provides a good agreement with CONTACT as far as the initial slope of the creep curve is concerned. However, the division of the slip and adhesion area does not coincide with CONTACT well in the presence of both lateral and longitudinal creep forces as discussed in [36].

As an alternative, a weighted mean of the flexibility parameters proposed by Kalker can be used to improve the separation of the slip and adhesion area but the agreement regarding the initial slope of the creep curve is decreased. The weighted mean flexibility parameter is given in the following form [13]:

$$L_0 = \frac{|\xi|L_\xi + |\eta|L_\eta + \sqrt{ab}|\varphi|L_\varphi}{\sqrt{\xi^2 + \eta^2 + ab\varphi^2}} \quad (7)$$

where  $\xi$ ,  $\eta$ , and  $\varphi$  are longitudinal, lateral and spin creepages. According to Archard's equation, wear occurs only in the slip area of the contacting surface. It means the division of the slip and adhesion area is more important than the initial slope of the creep curve for the wear calculation. Therefore, equation (7) is expected to be more suitable than equation (6) when FASTISM is applied for wear calculation. Numerical experiments are performed in Section 3 to see the effect of this assumption.

In steady state conditions the relative slip  $s(x, y)$  associated with a generic point  $(x, y)$  within the contact area is given by the following equation:

$$s(x, y) = w(x, y) - \frac{\partial u(x, y)}{\partial x} \quad (8)$$

where  $w(x, y)$  is the rigid slip which is defined as the ratio between the local velocity of one body relative to the other and the rolling velocity of the wheel expressed as follows:

$$w(x, y) = [\xi - y\varphi, \eta + x\varphi]^T \quad (9)$$

It can be seen from equation (8) that the slip velocity consists of two parts coming from the relative rigid motion represented by the first term and from the deformation of the

contacting surfaces reflected by the second term. For simplicity, the elastic contribution to the slip may be neglected [9]. Nevertheless, this contribution has been shown to be significant at least in case of large spin or partial slip contact [11]. The elastic contribution can be approximated according to equation (5). The contact patch is discretised using a rectangular grid with the size of  $\Delta x \times \Delta y$ , the following relation holds:

$$\frac{\partial u(x,y)}{\partial x} = L \frac{\partial \tau(x,y)}{\partial x} \approx L \frac{\tau(x,y) - \tau(x-\Delta x,y)}{\Delta x} \quad (10)$$

where  $\tau(x-\Delta x, y)$  represents the shear stress in the previous point of the contact area.

To determine the division of the slip and adhesion region within the contact area, Coulomb's friction law is locally applied at each cell of the contact patch. A boundary of the shear stress (also known as the traction bound) is formed as the production of the pressure and the coefficient of friction  $f$ :

$$g(x, y) = fp(x, y) \quad (11)$$

According to the FASTSIM algorithm, the slip and adhesion areas are determined as follows:

$$\text{in adhesion area: } |\mathbf{s}|=0, |\boldsymbol{\tau}| \leq g \quad (12)$$

$$\text{in slip area: } |\mathbf{s}|>0, |\boldsymbol{\tau}| = -g\mathbf{s}/|\mathbf{s}| \quad (13)$$

From equations (8)-(13), the magnitude of the velocity in the slip area can be calculated as follows:

$$\begin{aligned} v(x, y) &= V_0 |\mathbf{s}(x, y)| \\ &= V_0 \left( |\mathbf{w}(x, y)| - L \frac{\partial g(x, y)}{\partial x} \right) \\ &\approx V_0 \left( \sqrt{(\xi - y\varphi)^2 + (\eta + x\varphi)^2} - Lf \frac{p(x, y) - p(x - \Delta x, y)}{\Delta x} \right) \end{aligned} \quad (14)$$

It can be seen that if the traction bound is a semi-ellipse resulting from the contact pressure multiplied by the coefficient of friction, it prevents slip at the leading edge of the contact area [17] and the slip velocity goes to infinity at the trailing edge. To overcome this numerical issue, a parabolic traction bound is applied in the original FASTSIM algorithm as follows:

$$g(x, y) = \frac{2\mu N}{\pi ab} \left( 1 - \left( \frac{x}{a} \right)^2 - \left( \frac{y}{b} \right)^2 \right) \quad (15)$$

By substituting equation (15) to equation (14), it can be found that the parabolic traction bound leads to a linearly increasing slip velocity from the leading edge to the trailing edge of the contact area. Discussions on the choice of the traction bound and the corresponding influence on the creep force estimation and shear stress estimation can be found in [17,36].

In this paper, we focus on its influence on the slip velocity estimation and eventually on the wear prediction over the contact area.

### 3. Results and discussions

As mentioned above, a reliable method should be applied for the evaluation of the contact pressure and the slip velocity over the contact area in order to correctly determine the wear coefficient and eventually the wear distribution. In this section, slip velocity and the wear coefficient are investigated respectively in the current section with the attempt to assess the most suitable modelling method for wear based on Archard's equation.

#### 3.1 Contact pressure evaluation

As mentioned before, a comprehensive investigation into the impact of non-Hertzian contact modelling in wheel wear simulation performed by Enblom and Berg [15] indicates that the wear distribution obtained by CONTACT over non-elliptic patches significantly differs from the Hertz solution. The reason for the differences is mainly due to the influences of the different contact pressure distribution and the contact shape. Although the non-Hertzian contact model is necessary for a reliable wheel profile wear calculation, Hertzian model is used to investigate the influence of other parameters involved in wear simulation for its simplicity since the conclusion is applicable to both cases.

#### 3.2 Slip velocity evaluation

As stated in Section 2, the traction bound  $g$  and the flexibility  $L$  used in the FASTSIM algorithm influence the slip velocity distribution. Various approaches addressed in Section 2 will be assessed by taking CONTACT software [37] as the reference. The case studies reported in [38] are chosen and extended with pure creep cases as listed in Table 1 where cases 1-5 represent the tread contact and case 6 represents the flange contact condition according to the reference paper.

Table 1. Simulation condition for a single contact patch, extended from [38]

Quantity	Case 1	Case 2	Case 3	Case 4	Case 5	Case 6
$a$ [mm]	6.1	6.1	6.1	6.1	6.1	8.1
$b$ [mm]	8.5	8.5	8.5	8.5	8.5	4.2
$f$ [-]	0.3	0.3	0.3	0.3	0.3	0.5
$\xi$ [-]	0	-0.94e-3	-0.94e-3	-4×0.94e-3	-0.94e-3	-4.1e-3
$\eta$ [-]	0	-0.22e-3	0	0	-0.22e-3	3.1e-3
$\phi$ [m <sup>-1</sup> ]	0.29	0	0	0	0.29	1.2
$V_0$ [m/s]	44	44	44	44	44	22
$N$ [kN]	93	93	93	93	93	89

Similar results can be expected for the pure translational creepage condition since  $L_\xi$  and  $L_\eta$  are approximately equal. Therefore, a pure spin and combined translational creepage condition presented by case 1 and 2 in Table 1 are chosen to investigate the effect of the flexibility parameter on the calculation of the slip velocity. The parabolic traction bound is applied for the FASTSIM algorithm for these two cases. For the pure spin creepage

condition, the deviations mainly result from the difference between  $L_\phi$  and  $L_\xi$  or  $L_\eta$  as shown in Fig.5. The results from FASTSIM with different choice of flexibility parameter along with the reference results from CONTACT are shown in Figs 5 and 6.

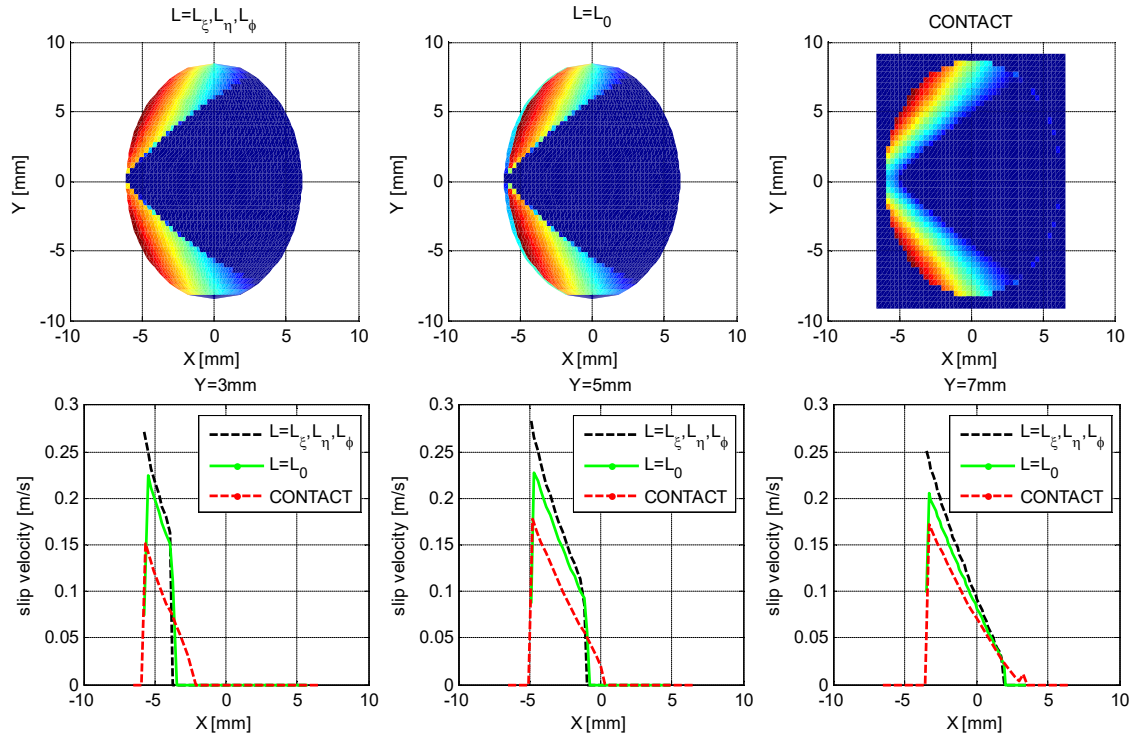
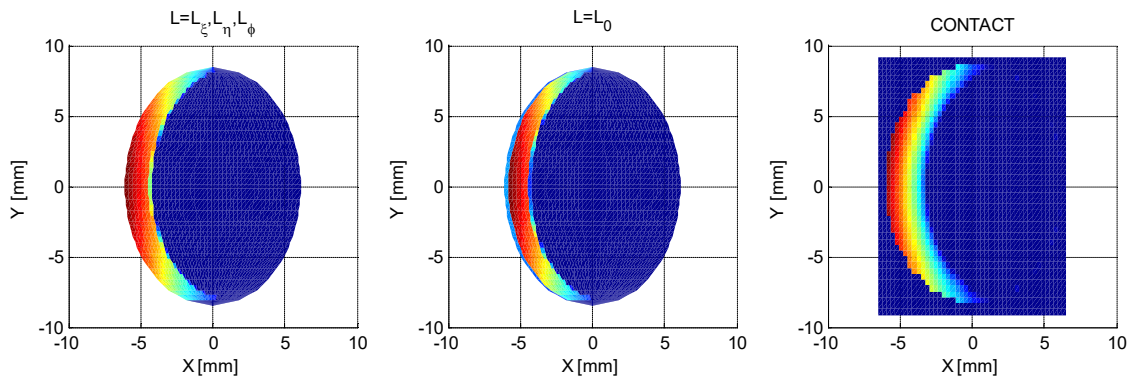


Fig.5 Top view of the slip velocity distribution obtained by FASTSIM with a single flexibility parameter (top left), FASTSIM with three flexibility parameters (top middle), and CONTACT (top right); and the slip velocity distribution over strip Y=3, 5 and 7 mm under pure spin condition (case 1).



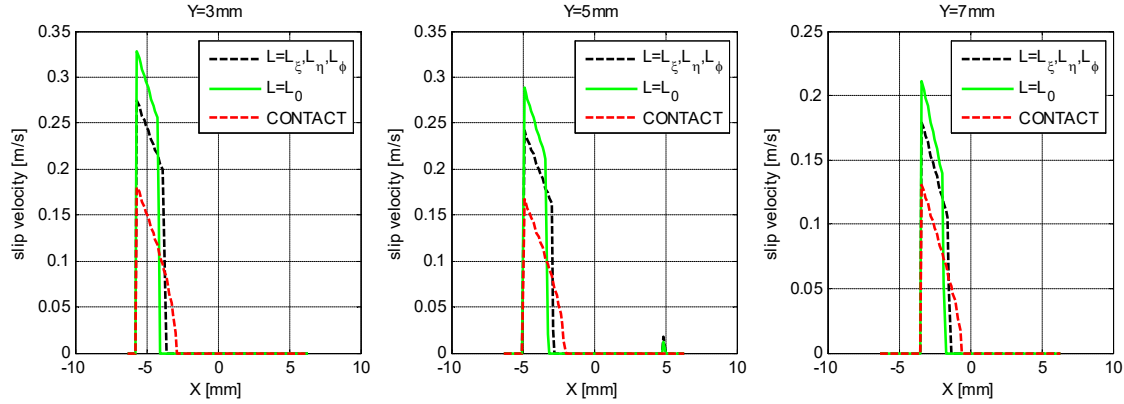


Fig.6 Top view of the slip velocity distribution obtained by FASTSIM with a single flexibility parameter (top left), FASTSIM with three flexibility parameters (top middle), and CONTACT (top right); and the slip velocity distribution over strip Y=3, 5 and 7 mm under combined translational creepage condition (case 2).

The results shown in Figs 5 and 6 suggest that the area of slip is underestimated by FASTSIM whereas the magnitude of the slip velocity is overestimated compared to CONTACT. Moreover, it can be seen from Fig.5 that FASTSIM with three flexibility parameters generates higher slip velocity close to the trailing edge of the contact area than that of FASTSIM with a single flexibility parameter which is in relatively good agreement with CONTACT under the pure spin condition. In contrast, FASTSIM with three flexibility parameters shows better agreement with CONTACT in terms of the slip velocity distribution over the entire slip area in the case of the combined creepage condition (case 2) as reported in Fig.6. Considering the combined creepage condition is dominant in the wheel-rail contact in practice, three flexibility parameters are used to calculate the slip velocity in FASTSIM i.e. equation (19), for further study in this work.

To investigate the influence of the traction bound on the slip velocity estimation in FASTSIM, the pure longitudinal creepage contact condition shown in case 3 is selected to perform the comparison. As mentioned in Section 2, the elliptic traction bound applied in FASTSIM results in a singularity in the slip velocity on the trailing edge of the contact area, which can be avoided by approximating the derivatives by means of finite differences. However, it gives rise to the dependency of the maximum slip velocity on the discretisation as shown in Fig.7.

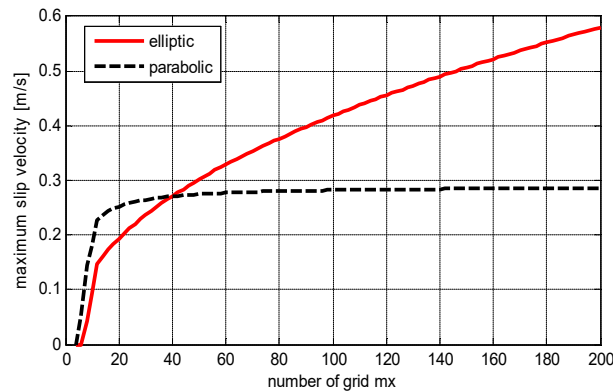


Fig.7 Maximum slip velocity as function of number of cells in the grid

The result shown in Fig.7 for case 3 proves that the maximum slip velocity over the contact area (on the trailing edge) is varied with the density of mesh when FASTSIM is used with an elliptic traction bound due to the singularity discussed in Section 2.3. From Fig.7, it also can be seen that the solution converges when the number of grid points is larger than 40 for the parabolic traction bound condition. It should be noted that a significantly overestimated slip velocity seems to be wrong, but it does not have a large effect on wear calculation as long as it is restricted to a tiny area of the contact patch. The slip velocity distributions over strips were calculated by FASTSIM with elliptic and parabolic traction bounds and CONTACT, respectively, for case 3. The slip velocities on the strips of  $Y=0$ , 4 and 8 mm are shown in Fig.8.

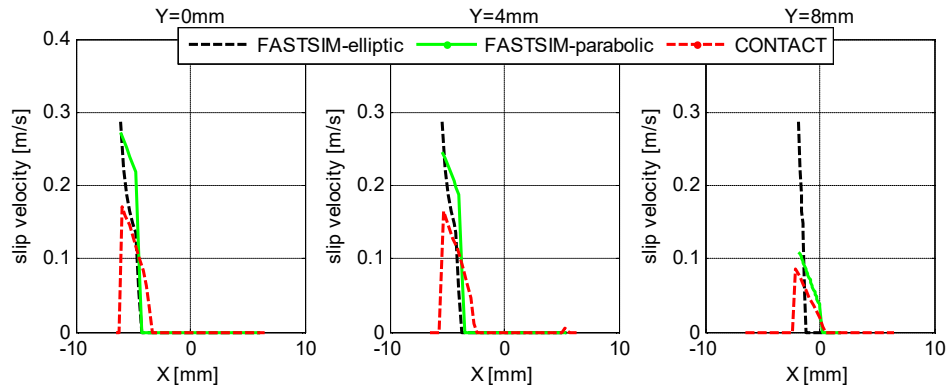


Fig.8 Slip velocity distribution over strip  $Y=0$ , 4 and 8 mm under pure longitudinal creepage condition (case 3).

It can be observed from Fig.8 that the slip velocity on the trailing edge is the same on different strips for FASTSIM with an elliptic traction bound because the same number of grid points in lateral and longitudinal directions is used within the contact patch, which leads to the grid spacing  $\Delta x$  varying per grid line and the same distribution at the same (relative) position. The maximum slip velocity varies with strip for FASTSIM with parabolic traction bound and CONTACT, and the adhesion-slip boundary estimated by FASTSIM with parabolic traction has better agreement with CONTACT. Moreover, the same conclusion as drawn from Figs 5 and 6 is found that FASTSIM overestimates the slip velocity compared with the reference provided by CONTACT.

It can be concluded based on the analysis above that three flexibility parameters combined with a parabolic traction bound in FASTSIM provides better agreement to CONTACT in terms of the estimate of the slip velocity distribution.

### 3.3 Power density evaluation

For reasons of consistency in the simplified theory, an unrealistic paraboloidal normal contact pressure is generally used instead of the semi-ellipsoidal form obtained by the Hertz theory when a parabolic traction bound is applied [39]. This means that the traction bound influences not only the slip velocity distribution as discussed above but also the pressure distribution in the original FASTSIM. According to Archard's equation, the contact pressure in the slip area also influences the wear. Therefore, it is necessary to

investigate the influence of the choice of normal pressure form on wear estimation. To this end, the power density defined by the product of the contact pressure and the slip velocity is calculated with different contact pressure distributions for comparison.

For the following calculations, the traction bound is assumed to be parabolic, but the contact pressure is assumed to be semi-ellipsoidal and paraboloidal, respectively in the FASTSIM algorithm implemented here. The comparisons are shown in Fig.9 and Fig.10. The legend N.ell+FASTSIM-T.par stands for the ellipsoidal normal pressure distribution and a parabolic traction bound used in FASTSIM and N.par+FASTSIM-T.par denotes the paraboloidal normal pressure distribution and a parabolic traction bound used in FASTSIM which is obtained by multiplying the normal pressure by the coefficient of friction.

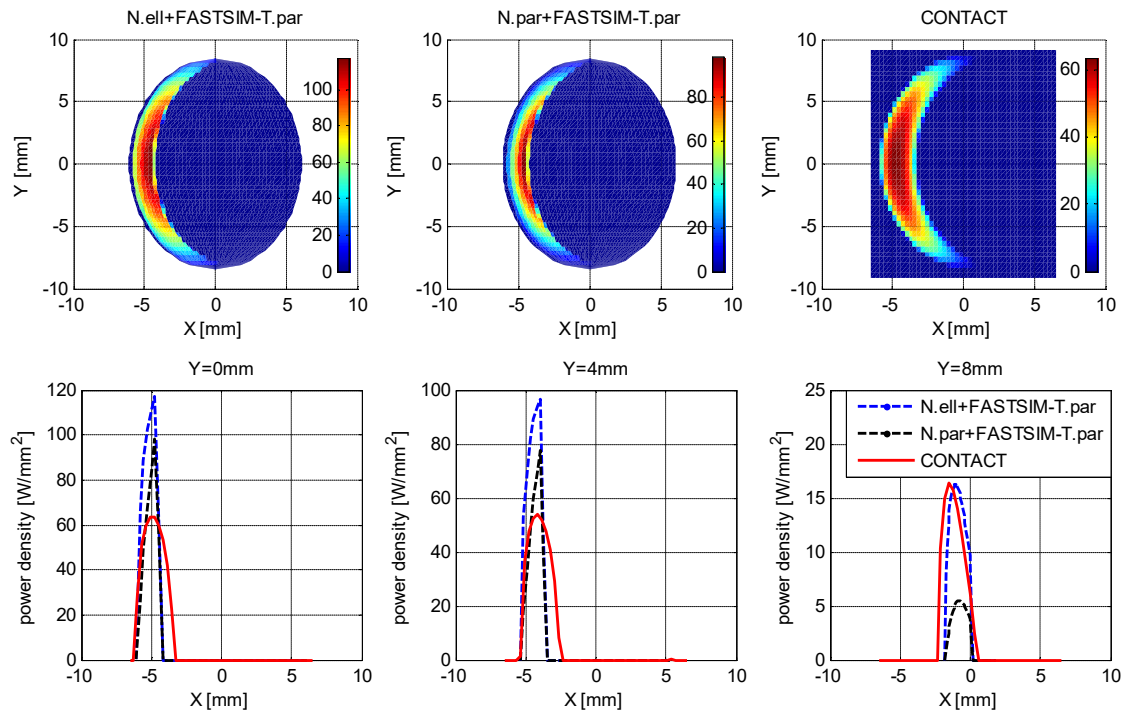


Fig.9 Power density distribution on the contact patch obtained by different methods (top), and its variation over the strips of  $Y=0, 4$  and  $8$  mm (bottom) for low longitudinal creepage presented in case 3.

It can be observed from Fig.9 that the slip area is underestimated by FASTSIM with a parabolic traction bound compared with CONTACT, and the power density over the slip area estimated by FASTSIM with a semi-ellipsoidal contact pressure is higher than that by FASTSIM with a paraboloidal pressure distribution for the low longitudinal creepage condition because the semi-ellipsoidal pressure is larger than the paraboloidal pressure in the region  $\frac{\sqrt{7}}{4}x_l < x < x_l$  ( $x_l$  is the edge of the contact area).

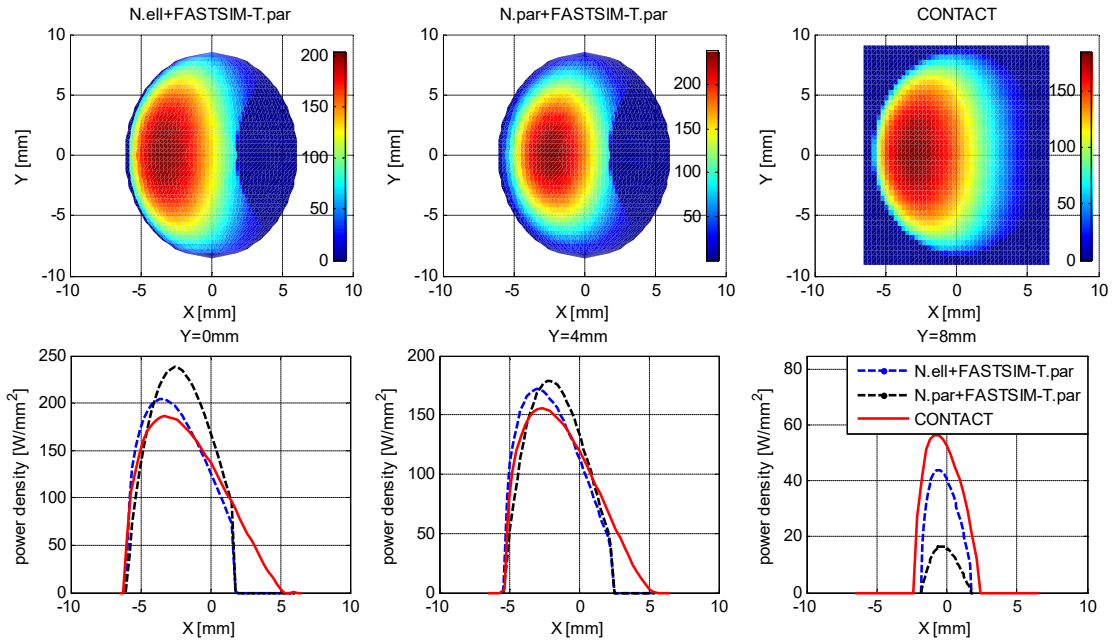
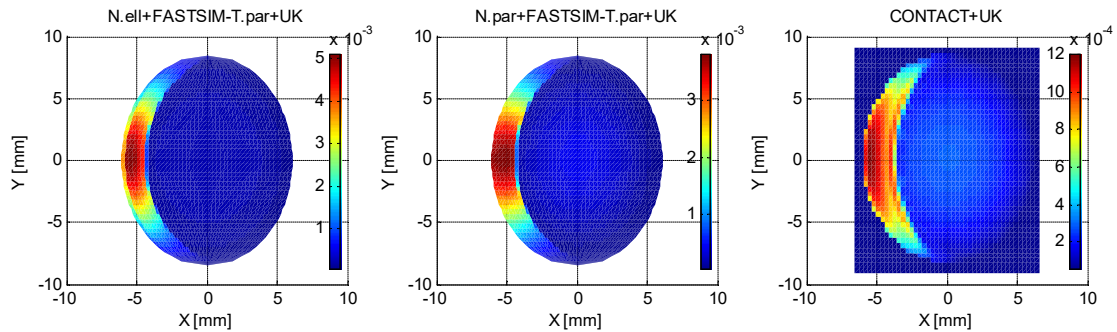


Fig.10 Power density distribution on the contact patch obtained by different methods (top), and its variation over the strips of  $Y=0,4$  and  $8$  mm (bottom) for high longitudinal creepage presented in case 4.

It can be observed from Fig.10 that the distribution of the power density calculated by the different methods is similar, but the results obtained by FASTSIM with a semi-ellipsoidal pressure are in better agreement with CONTACT compared to the paraboloidal pressure for the high longitudinal creepage condition.

### 3.3 Wear coefficient evaluation

The wear coefficient is determined by the two methods presented in Section 2, namely the UK and MV method for comparison. The slip velocity and pressure distribution that are required to determine the wear coefficient were calculated by FASTSIM with different traction bound and by CONTACT, respectively. The rail material BS11 is chosen for the UK method in the calculation. The two cases 3 and 4 discussed above are chosen to demonstrate the differences, and the results are shown in Figs.11 and 12.



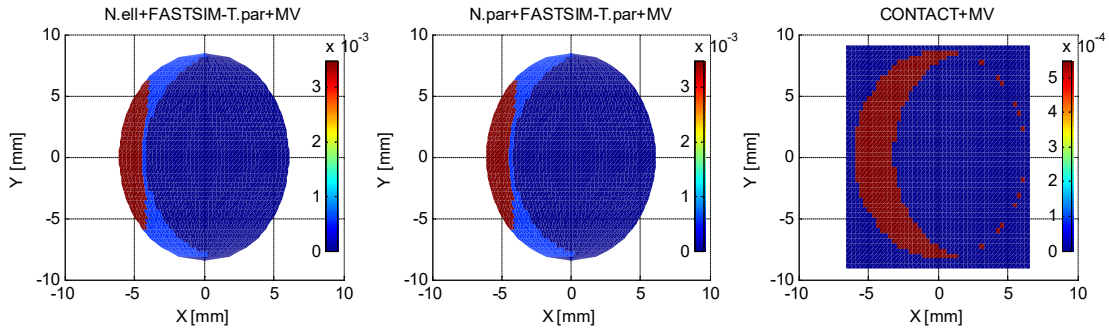


Fig.11 Wear coefficient distribution on the contact patch determined by the UK method (top) and the MV method (bottom) in different contact modelling algorithms for case 3.

For the low longitudinal creepage case shown in Fig.11, the distribution of the wear coefficient determined by the UK and MV method is significantly different regardless of the algorithm used for contact modelling. There is no surprise for these results because the UK method here is applied to a specific material pair i.e. class D/BS11 whereas the MV method is designed to be material independent. The results obtained by the UK method is smooth, in contrast to discontinuous results of the MV. Moreover, the result is varied with different contact models when the UK method is used to determine the wear coefficient. In detail, FASTSIM overestimates the wear coefficient with respect to CONTACT. The influence is marginal between FASTSIM with different contact pressure forms when the MV method is used because the maximum pressure in the slip area falls in the same region of Fig.2.

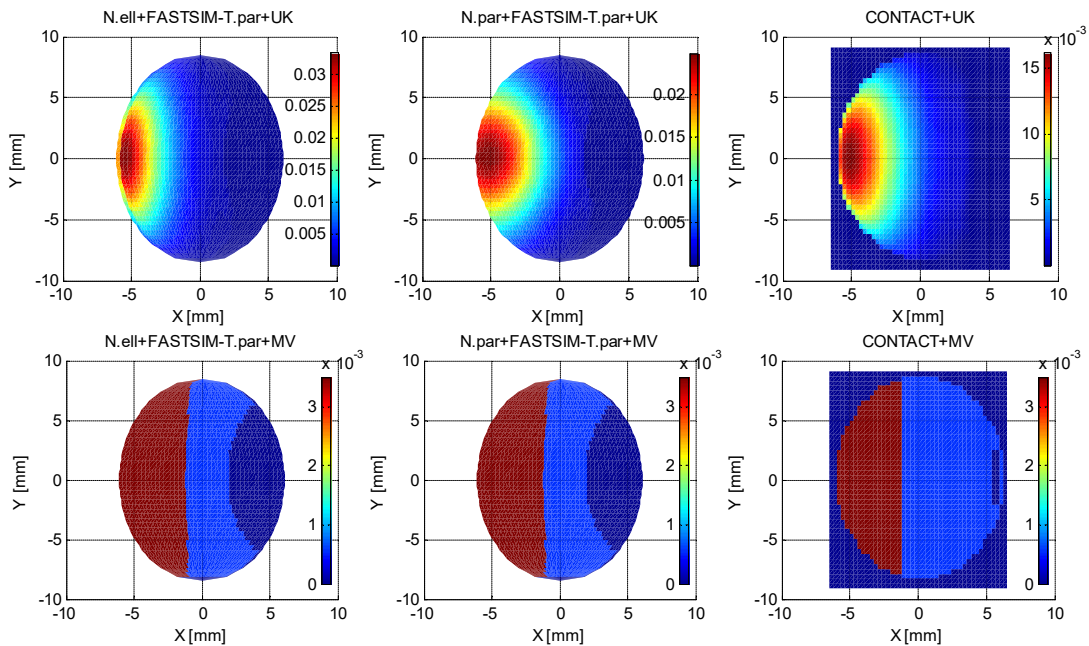


Fig.12 Wear coefficient distribution on the contact patch determined by the UK method (top) and the MV method (bottom) in different contact modelling algorithms for case 4.

It can be concluded for case 4 that the pattern of the wear coefficient distribution predicted by FASTSIM and CONTACT is similar and continuous when the UK method is applied whereas the maximum value calculated by FASTSIM is approximately three times higher

than that by CONTACT, which is mainly due to the overestimated slip velocity by FASTSIM as discussed in Section 3.2. In contrast, when the MV method is used the distribution of the wear coefficient is different for each one of the considered contact models. The same value for each region in the wear coefficient distribution map is due to the discontinuous KTH map used in the MV method. It is interesting to note that the maximum value of the wear coefficient determined by the UK method with CONTACT is similar to the one provided by the MV method.

### 3.5 Wear depth evaluation

The wear depth distributions over the contact patch for cases 5 and 6 which stand for the tread contact and flange contact, respectively, were calculated according to equation (3) by different methods for contact modelling and wear coefficient determination.

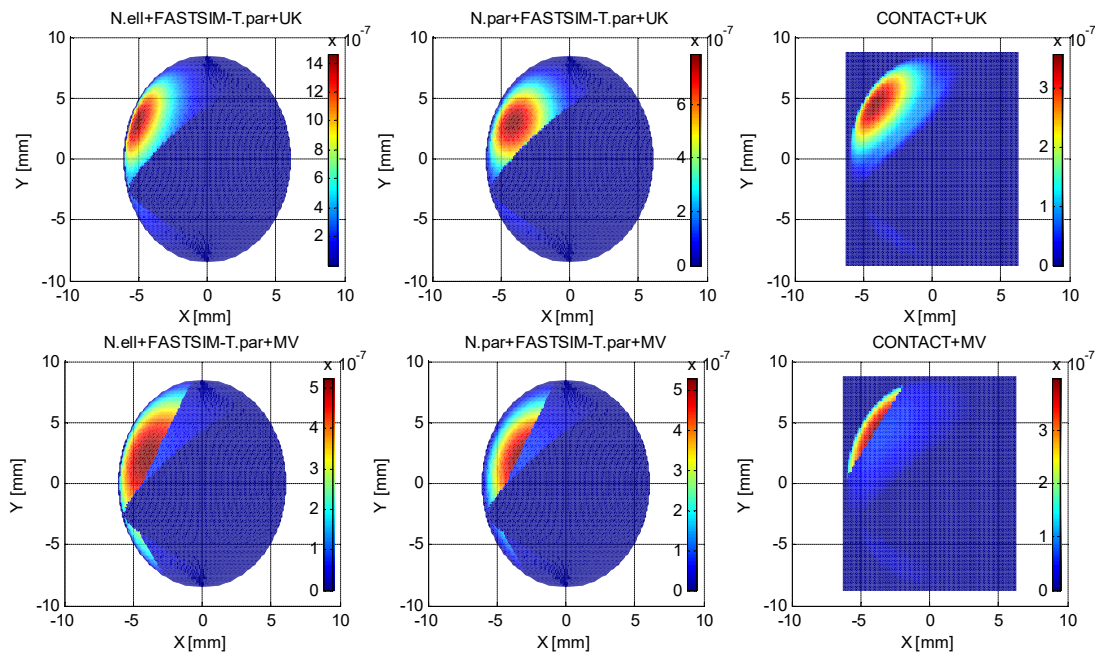


Fig.13 Wear depth distribution on the contact patch determined by the UK method (top), the MV method (bottom) in different contact modelling methods for case 5.

Fig. 13 shows the colour map of the wear distribution estimated by different approaches. It can be observed that the pattern of the wear distribution over the contact patch is similar for different contact models when the UK method is used to determine the wear coefficient, but the magnitude differs significantly. In contrast, the distribution pattern of the wear is different for different contact models with the same level of magnitude due to the discontinuous map used in the MV method to determine the wear coefficient.

In order to have a clear insight into the influences caused by the contact modelling method and the wear coefficient determination method on the wear estimation, the wear variation over strips is taken from the contact patch for comparison as shown in Figs. 14 and 15.

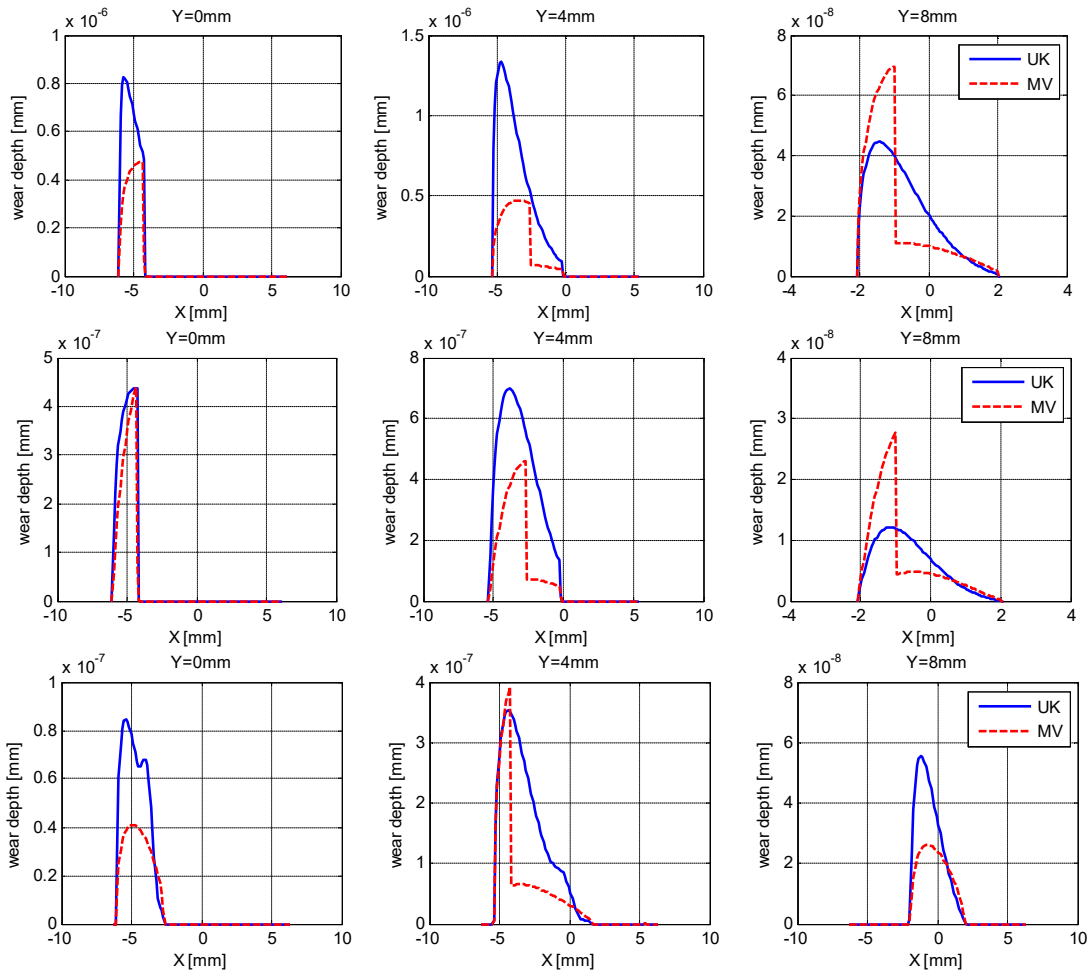
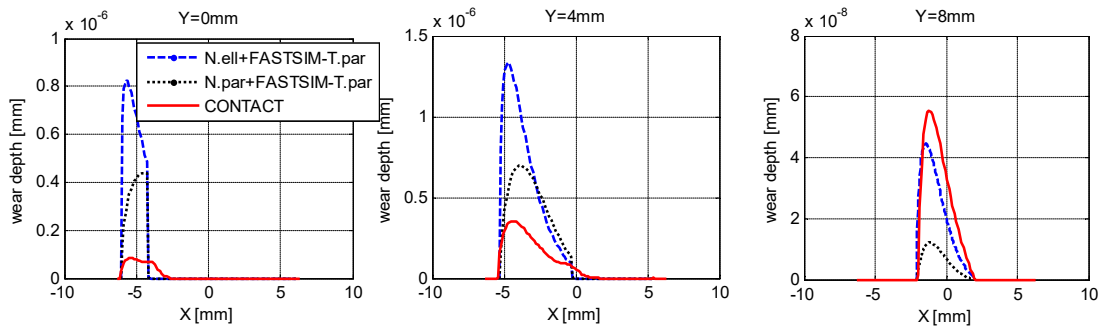


Fig.14 Comparison of the wear depth over strips  $Y=0, 4$  and  $8$  mm calculated with (top) FASTSIM combined with ellipsoidal contact pressure, (middle) FASTSIM combined with paraboloidal contact pressure and (bottom) CONTACT for case 5 (tread contact).

It can be observed from Fig.14 that the wear estimated with the UK method differs from that of the MV method not only in magnitude but also for the distribution pattern in most contact region regardless of the contact modelling method. Generally, the UK method overestimates the wear compared to the MV method.



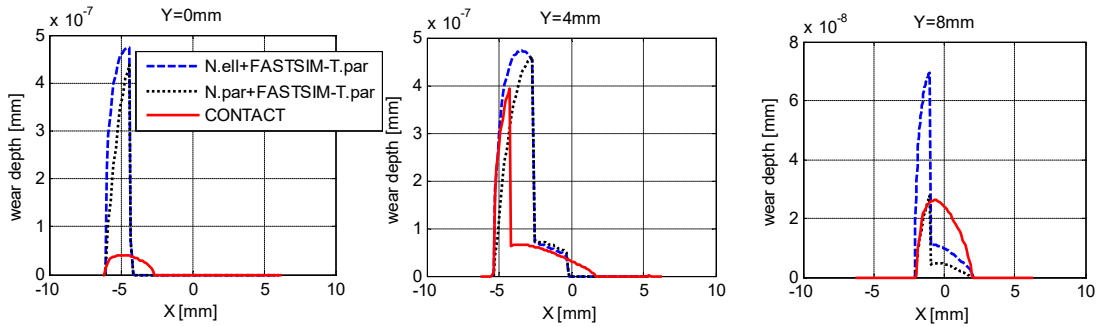


Fig.15 Comparison of the wear depth over strips  $Y=0, 4$  and  $8$  mm calculated with (top) UK method and (bottom) MV method for case 5 (tread contact).

It can be observed from Fig.15 that the influence of the contact modelling method on wear is more significant when the UK method is used to determine the wear coefficient. Moreover, FASTSIM overestimates the wear compared with CONTACT for most part of the contact area, and the highest wear depth is predicted by FASTSIM when an ellipsoidal contact pressure is assumed.

As for the tread contact case 5, the same analysis procedure is followed by the flange contact case 6.

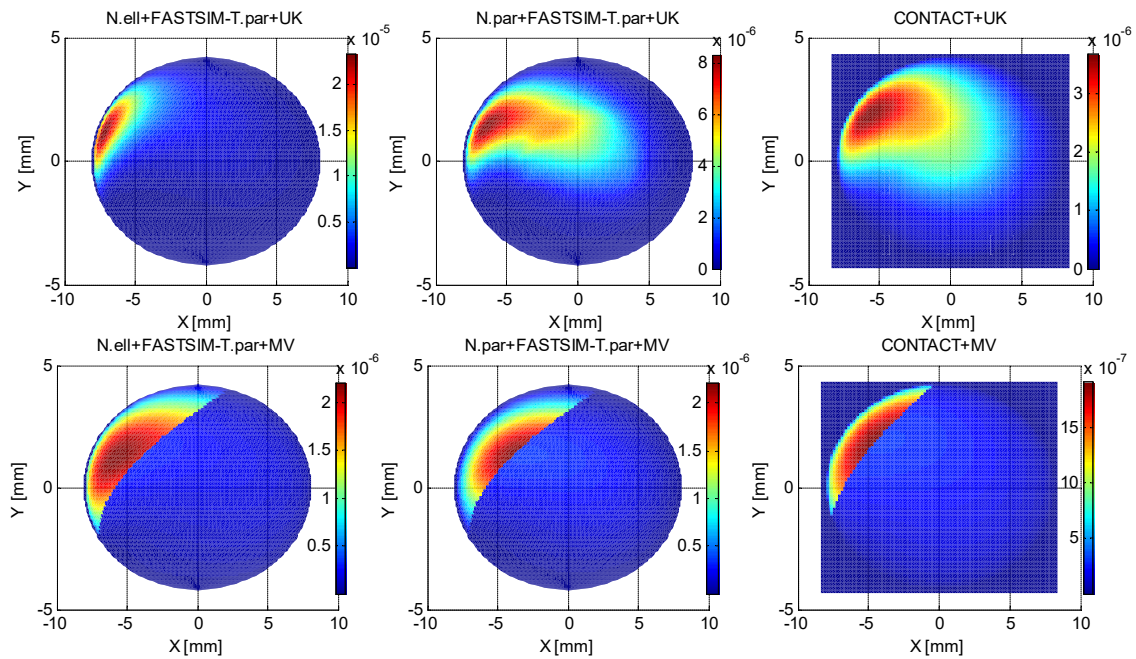


Fig.16 Wear depth distribution on the contact patch determined by the UK method (top), the MV method (bottom) in different contact modelling methods for case 6 (flange contact).

Different from the tread contact condition shown in Fig.15, the pattern of the wear distribution over the contact patch obtained by FASTSIM combined with an ellipsoidal contact pressure differs from the results obtained with a paraboloidal pressure and CONTACT when the UK method is used to determine the wear coefficient. However, the wear distribution pattern is similar for different contact models when the MV method is

used to determine the wear coefficient.

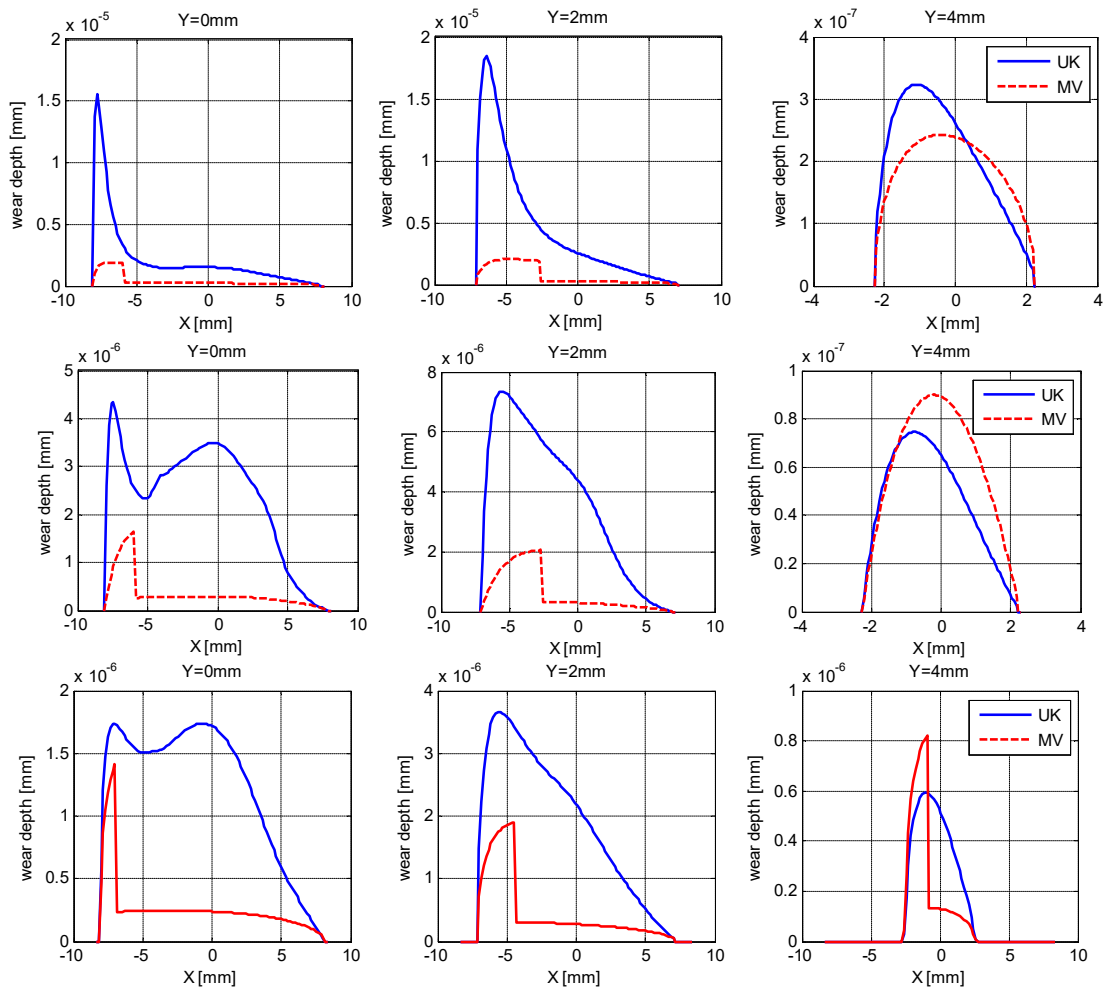


Fig.17 Comparison of the wear depth over strips Y=0, 2 and 4 mm calculated with (top) FASTSIM combined with ellipsoidal contact pressure, (middle) FASTSIM combined with paraboloidal contact pressure and (bottom) CONTACT for case 6 (flange contact).

Similar conclusions can be drawn from Fig.17 as for the tread contact condition shown in Fig.14 that the method to determining the wear coefficient has a considerable influence on the wear depth predicted. In more detail, the UK method generally overestimates the wear compared with the MV method regardless of the contact modelling method, and the results obtained with the UK method are smoother along the rolling direction of the contact patch.

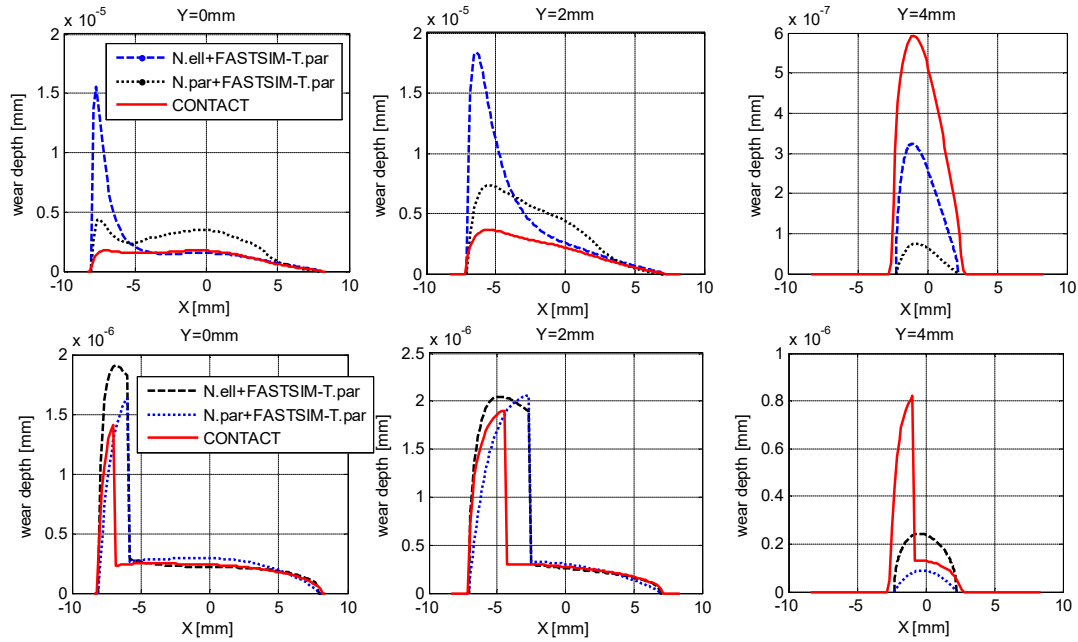
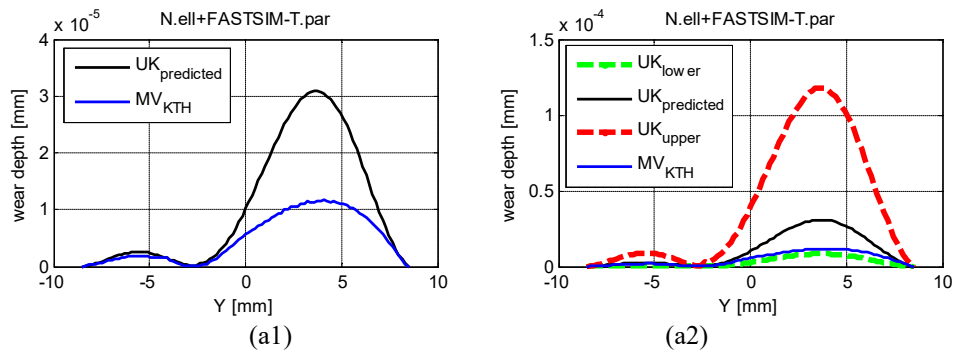


Fig.18 Comparison of the wear depth over strips  $Y=0, 4$  and  $8$  mm calculated with (top) UK method and (bottom) MV method for case 6 (flange contact).

From Fig.18, the same conclusion can be drawn as for Fig.15 in terms of the effect of the contact modelling and wear coefficient on the wear. It should be noted that the smooth wear distribution in the contact area predicted by the UK method is more realistic and useful for further damage analysis.

It should be noted that the final outcome of the wheel wear procedure is the updated wear profile considering the effect of material removal which is generally presented as the wear depth over the contact patch in lateral direction. To obtain this quantity, the wear distribution over each contact patch is calculated by adding the wear depths for each element in the slip zone for all longitudinal strips of the contact patch. The corresponding results for cases 5 and 6 are shown in Figs 19 and 20, respectively.



(a1)

(a2)

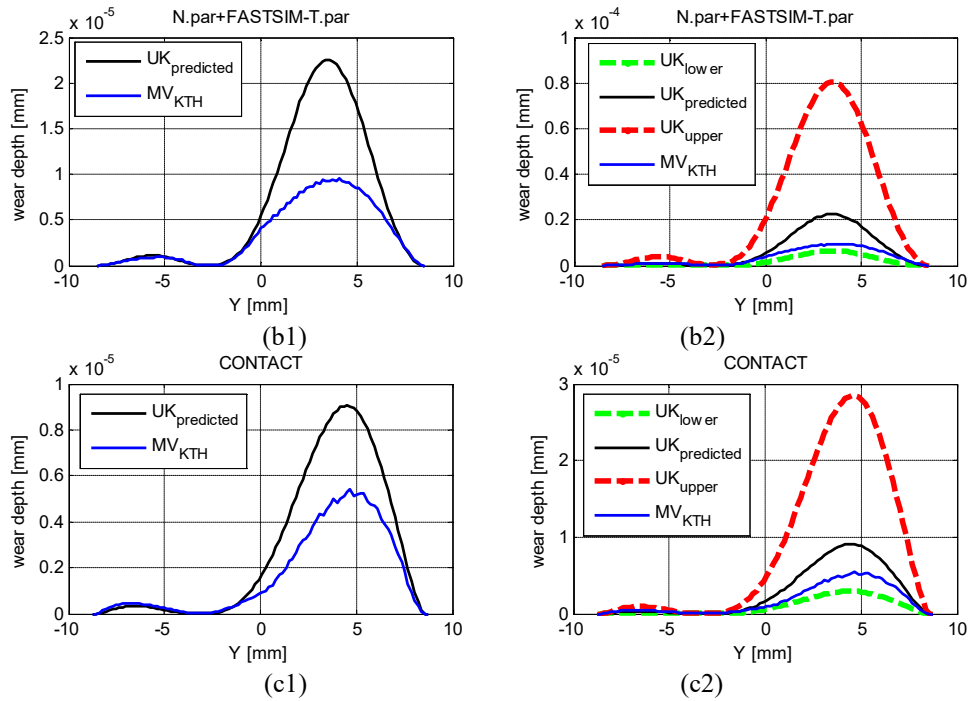
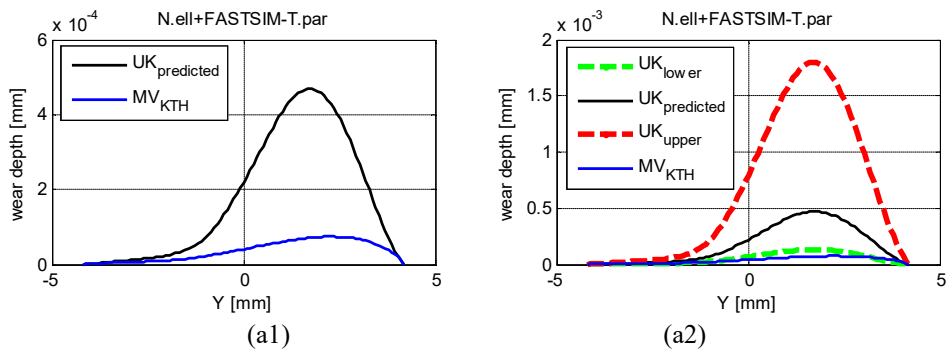


Fig.19 Wear depth distribution along the y-axis calculated in various methods (a1-c1) without boundaries of the UK method and with the boundaries (a2-c2) for case 5 (tread contact).

It can be concluded from Fig.19 that when the UK method is used to determine the wear coefficient, the wear calculation result contains more information including the predicted wear depth and its upper and lower boundaries. In contrast, a single determinate result is provided by the MV method. The similar wear distribution over the y-axis can be obtained by the UK and MV method, and the same positions of peaks are predicted. However, the maximum value of wear depth calculated by the UK method is much higher than the one provided by the MV method for this specific materials combination. In terms of the effect of the method used to perform the local contact analysis, CONTACT estimates lowest wear and FASTSIM with an elliptical contact pressure estimates highest wear in this case.



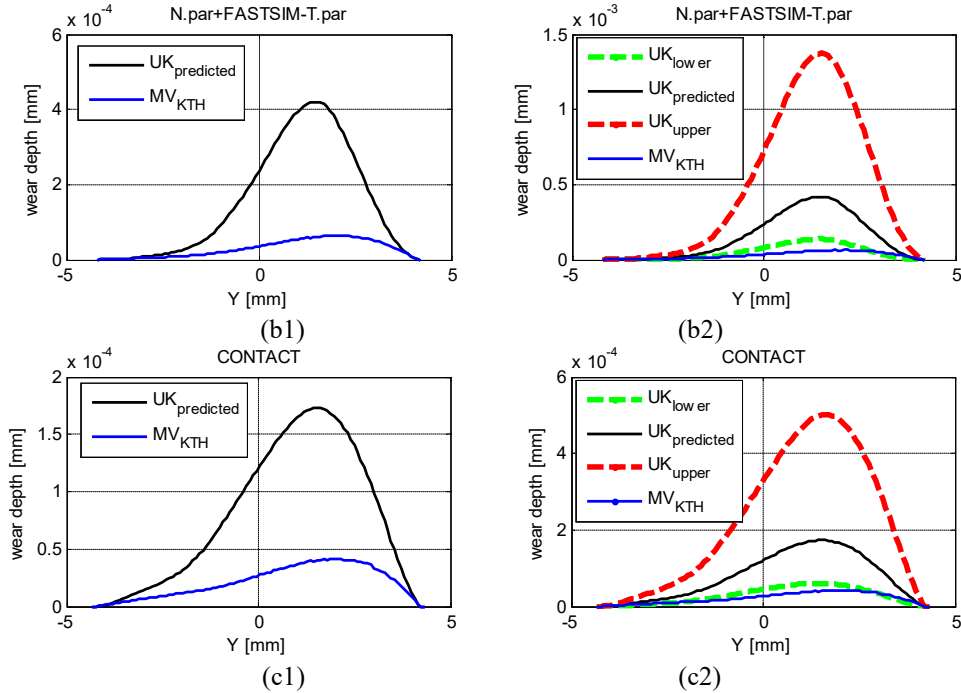


Fig.20 Wear depth distribution along the y-axis calculated in various methods (a1-c1) without boundaries of the UK method and with the boundaries (a2-c2) for case 6 (flange contact).

For the flange contact condition shown in Fig.20, the wear predicted by the UK method is much higher than that by the MV method, and the peak position is different. The wear depth estimated by CONTACT is lowest compared with other contact modelling method.

It can be concluded that the commonly used MV method for determination of the wear coefficient must be calibrated for any specific application. The UK method can be applied for a specific case with required measurement available and it is able to provide a min-max range for wear estimation instead of a deterministic value as the currently used MV method. The UK method is more sensitive to the contact modelling method compared to the MV method for wear estimation, and the FASTSIM algorithm generally overestimates the wear compared with CONTACT.

Although the conclusions drawn above are based on the elliptic contact conditions, they can be applied to the non-Hertzian contact condition as in the commonly used approximate non-Hertzian contact modelling methods, e.g. Kik-Piotrowski method [32] the pressure distribution along the rolling direction is assumed to be semi-elliptic.

#### 4. Conclusions

The influence of the flexibility parameter and the traction bound used in the FASTSIM algorithm on the slip velocity and the wear distribution over the contact patch was investigated in this paper. The simulation results suggest that FASTSIM with a parabolic traction bound can provide better agreement to CONTACT in terms of the slip velocity distribution than an elliptic traction bound and using three flexibility parameters provides closer results to CONTACT in terms of the slip velocity distribution than the same case by

using a single flexibility parameter as far as a combined creepages condition is concerned.

A newly available approach (UK method) to determining the wear coefficient in Archard's equation based on the measurements considering its uncertainty was assessed by comparing with the commonly used method MV. This method provides a min-max range for wear estimation instead of a single deterministic value provided by the MV method. Furthermore, the UK method provides a more detailed wear distribution over the contact patch for further damage analysis. It should be noted that the UK method was implemented based on limited measured data, therefore the availability of a larger set of measured data covering a wider range of contact conditions is desirable to extend the assessment of the applicability of the UK method and to improve its accuracy.

The FASTSIM algorithm overestimates the slip velocity and wear with reference to CONTACT especially when the UK method is used to determine the wear coefficient for all the cases considered. An elaborate contact model e.g. CONTACT combined with a fine wear coefficient determination method, e.g. the UK method, is able to offer a more realistic wear prediction compared to the methods presently used for wheel wear estimation in railway vehicles.

## Acknowledgements

The authors would like to thank Dr Edwin Vollebregt for fruitful discussions on contact mechanics.

## References

- [1] Chevalier, L., Eddhahak-Ouni, A., and Cloupet, S. "On a Simplified Model for Numerical Simulation of Wear During Dry Rolling Contacts." *ASME. J. Tribol.* January 2009; 131(1): 011402.
- [2] Lim SC, Ashby MF, Brunton JH. Wear-rate transitions and their relationship to wear mechanisms. *Acta Metall* 1987;35:1343–8.
- [3] A. Hugnell and S. Andersson, "Simulating follower wear in a cam-follower contact," *Wear*, vol. 179, no. 1-2, pp. 101–107, 1994.
- [4] I. El-Talji and E. Jantunen, "Dynamic modelling of wear evolution in rolling bearings," *Tribology International*, vol. 84, pp. 90–99, 2015.
- [5] T.G. Pearce, N.D. Sherratt, Prediction of wheel profile wear, *Wear* 144 (1991) 343–351.
- [6] I. Zobory, Prediction of wheel/rail profile wear, *Vehicle Syst. Dynam.* 28 (1997) 221–259.
- [7] F. Braghin, S. Bruni, F. Resta, Wear of railway wheel profiles: a comparison between experimental results and a mathematical model, *Suppl. Vehicle Syst. Dynam.* 37 (2002) 478–489.
- [8] F. Braghin, R. Lewis, R.S. Dwyer-Joyce, S. Bruni, A mathematical model to predict railway wheel profile evolution due to wear, *Wear* 261 (2006) 1253–1264.
- [9] T. Jendel, "Prediction of wheel profile wear-comparisons with field measurements," *Wear*, vol. 253, pp. 89–99, 2002.
- [10] T. Jendel and M. Berg, "Prediction of wheel profile wear," *Suppl. Veh. Syst. Dynam.*, vol. 37, pp. 502–513, 2002.
- [11] R. Enblom and M. Berg, "Simulation of railway wheel profile development due to wear influence of disc braking and contact environment," *Wear*, vol. 258, no. 7–8, pp. 1055–1063, 2005.

- [12] Saad M. S. Mukras, "Computer Simulation/Prediction of Wear in Mechanical Components", *Advances in Tribology*, vol. 2020, Article ID 8867351, 15 pages, 2020.
- [13] J. J. Kalker, "A Fast Algorithm for the Simplified Theory of Rolling Contact," *Veh. Syst. Dyn.*, vol. 11, no. 1, pp. 1–13, 1982.
- [14] J.J. Kalker, *Three-Dimensional Elastic Bodies in Rolling Contact*, Kluwer Academic Publisher, Dordrecht, 1990.
- [15] R. Enblom and M. Berg, "Impact of non-elliptic contact modelling in wheel wear simulation," *Wear*, vol. 265, no. 9–10, pp. 1532–1541, 2008.
- [16] G. Tao, Z. Wen, X. Zhao, X. Jin, "Effects of wheel–rail contact modelling on wheel wear simulation" *Wear*, 366-367:146-156, 2016.
- [17] E. A. H. Vollebregt and P. Wilders, "FASTSIM2: A second-order accurate frictional rolling contact algorithm," *Comput. Mech.*, vol. 47, no. 1, pp. 105–116, 2011.
- [18] R. Lewis and U. Olofsson, "Mapping rail wear regimes and transitions," *Wear*, vol. 257, no. 7–8, pp. 721–729, 2004.
- [19] S. M. Hsu and M. C. Shen, "Wear Maps," in *Modern Tribology Handbook. Vol 1*, B. Bhushan, Ed. Florida: CRC Press LLC, 2001.
- [20] Lewis, R., Dwyer-Joyce, R.S., Olofsson, U., Pombo, J., Ambrósio, J., Pereira, M., Ariaudo, C., Kuka, N., "Mapping Railway Wheel Material Wear Mechanisms and Transitions", *Journal of Rail and Rapid Transit*, Proceedings of the IMechE Part F, Vol. 224, pp125-137, 2010.
- [21] Y. Zhu, J. Sundh and U. Olofsson., "A Tribological View on Wheel-Rail Wear Maps", *International Journal of Railway Technology* 2(3):79-91, 2013.
- [22] N. A. C. Cressie, *Statistics for Spatial Data*, Revised ed. Wiley, 1993.
- [23] R. Holm, *Electric Contacts Handbook*, Springer, (H. Gerbers, Stockholm, 1946).
- [24] Archard, J.F. Contact and Rubbing of Flat Surfaces. *Journal of Applied Physics*, 1953, 24(8), 981-988.
- [25] J. Andersson, A. Almqvist, R. Larsson, Numerical simulation of a wear experiment, *Wear*, 271, 11-12, 2947-2952, 2011.
- [26] K. Kato and K. Adachi, "Wear Mechanisms," in *Modern Tribology Handbook. Vol 1*, B. Bhushan, Ed. Florida: CRC Press LLC, 2001.
- [27] J. Pombo, J. Ambrósio, M. Pereira, R. Lewis, R. Dwyer-Joyce, C. Ariaudo, and N. Kuka, "Development of a wear prediction tool for steel railway wheels using three alternative wear functions," *Wear*, vol. 271, no. 1–2, pp. 238–245, 2011.
- [28] Y. Jin, M. Ishida, and A. Namura, "Experimental simulation and prediction of wear of wheel flange and rail gauge corner," *Wear*, vol. 271, no. 1–2, pp. 259–267, 2011.
- [29] A. Bevan, P. Molyneux-Berry, B. Eickhoff, and M. Burstow, "Development and validation of a wheel wear and rolling contact fatigue damage model," *Wear*, vol. 307, pp. 100–111, 2013.
- [30] M. A. Cremona, B. Liu, Y. Hu, S. Bruni, and R. Lewis, "Predicting railway wheel wear under uncertainty of wear coefficient, using universal kriging," *Reliab. Eng. Syst. Saf.*, vol. 154, pp. 49–59, 2016.
- [31] T. Telliskivi and U. Olofsson, "Contact mechanics analysis of measured wheel – rail," *Proc. Inst. Mech. Eng. Part F- J. Rail Rapid Transit*, vol. 215, pp. 65–73, 2001.
- [32] W. Kik and J. Piotrowski, "A fast, approximate method to calculate normal load at contact between wheel and rail and creep forces during rolling," in *Proceedings of 2nd mini-conference on contact mechanics and wear of rail/wheel systems*, 1996, pp. 52–61.
- [33] J. Ayasse and H. Chollet, "Determination of the wheel rail contact patch in semi-Hertzian conditions," *Veh. Syst. Dyn.*, vol. 43, no. 3, pp. 161–172, 2005.
- [34] B. Liu, S. Bruni, and E. Vollebregt, "A non-Hertzian method for solving wheel–rail normal contact problem taking into account the effect of yaw," *Veh. Syst. Dyn.*, vol. 3114, no. June, pp. 1–21, 2016.

- [35]J. J. Kalker, “On the Rolling Contact of Two Elastic Bodies in the Presence of Dry Friction,” Delft University of Technology, 1967.
- [36]M. Sh. Sichani, R. Enblom, and M. Berg, “An alternative to FASTSIM for tangential solution of the wheel–rail contact,” *Veh. Syst. Dyn.*, vol. 54, no. 6, pp. 748–764, 2016.
- [37]E. A. H. Vollebregt, “User guide for CONTACT, Rolling and sliding contact with friction,” VORtech BV, Delft, 2015.
- [38]E. Roger and M. Berg, “Towards calibrated wheel wear simulation-a comparison between traditional approach and novel methods,” in *6th International Conference on Railway Bogies and Running Gears*, 2004, pp. 181–190.
- [39]J. J. Kalker, “Rolling Contact Phenomena : Linear Elasticity,” in *Proceedings of the CISM International Centre for Mechanical Sciences*, 2001, pp. 1–84.